Performance issues with photonic beamformers

Performance Issues with Photonic Beamformers

Invited Talk

M. Tur, L.Yaron, O.Raz* and R.Rotman
Tel Aviv University, Tel Aviv, Israel
e-mail: tur@eng.tau.ac.il, Tel: +972-3-6408125, Fax: +972-3-6405940

***Abstract* - A photonic beamformer is presented, having smooth behavior. Third-order nonlinearities, resulting from its opto-electronic components, are investigated, with emphasis on their impact on the contrast of imaging radars. This contrast is shown to be severely limited by the induced RF nonlinearities. Limitations on the allowable modulation index are studied for linearly-chirped pulses returned from clutter.**

***Index Terms* — photonic beamformers, delay-lines, nonlinearities, imaging radar.**

I. Introduction

Optical processing of microwave signals can be beneficial for microwave applications due to its inherent advantages, which include large bandwidth, low loss, EMI tolerance, and low weight and volume. Among the various applications studied, the use of photonics for controllable delay of microwave signals is one of the most promising areas. This technology enables the use of photonic components for two important practical applications: photonically based filtering of microwave signals and the implementation of optically fed phased-array antennas.

Several techniques have been proposed in order to implement optical delay lines including switching between various optical paths, wavelength conversion with dispersive media, dynamic gratings, and the modification of the group velocity (commonly referred to in the literature as “slow light"). Each of the mentioned techniques offers distinct advantages and drawbacks in terms of the achievable delay, tuning speed and accuracy, system simplicity and ease of control.

Regardless of the specific technique used to implement the optical delay, photonic beamformers exhibit extremely wide bandwidth and large scan angles, far superior to those achieved by traditional RF schemes. However, with their advantages in mind, photonic beamformers still need to satisfy quite stringent performance requirements, such as a very smooth RF to RF transfer function, low noise figure and linear operation. Alas, most electronic to optical converters and some of the optical to electronic converters exhibit nonlinear behavior, significantly contributing to nonlinear budget of the link. In this paper we demonstrate highly smooth behavior of an implemented beam former and investigate the effects of third-order nonlinearities, resulting for example from Mach-Zehnder modulators, on photonic beamformers in general, and especially on the contrast of imaging radars. This contrast is shown to be severely limited by RF nonlinearities introduced by the optical components. Limitations on the allowable modulation index are studied for linearly-chirped pulses returned from clutter.

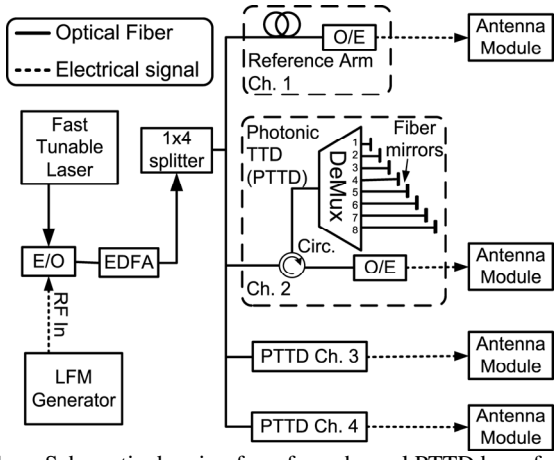

Fig. 1. Schematic drawing for a four-channel PTTD beamformer. [5] © 2008,IEEE

II. WDM Based Photonic Beamformer with Smooth RF Response

Previously [6], we have described a wavelength-Controlled Photonic True Time Delay (PTTD) module, having excellent RF characteristics. The smooth RF transfer function of the PTTD unit was achieved by using a passive design, based on wavelength-controlled routing of the signal through different optical paths. Based on this building block and a fast tunable laser, a four channel photonic beamformer was built, exhibiting a very smooth RF response in both the C and X bands, high uniformity between the RF transfer function of different channels, sub microsecond tuning speed and a single point of control.

The four channel beamformer is shown in Fig. 1.

Light coming from the fast tunable laser was double-sideband modulated by the RF source, using an in-quadrature biased Mach-Zehnder, electrical to optical (E/O) converter. The modulated light was then amplified and evenly split among the four channels. Channel 1 served as a reference, comprising only a length of fiber, and the other three channels

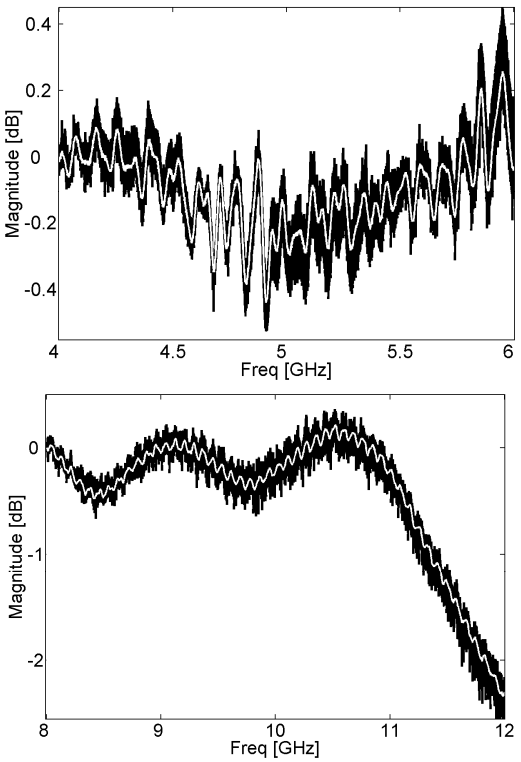

Fig. 2. The measured frequency dependence of the magnitude of S_{21} (after its frequency-averaged value has been subtracted) for all four channels at all eight wavelengths, resulting in 32 superimposed curves. The white line is the per-frequency mean, and most of the C and X microwave bands is covered. [5] © 2008,IEEE.

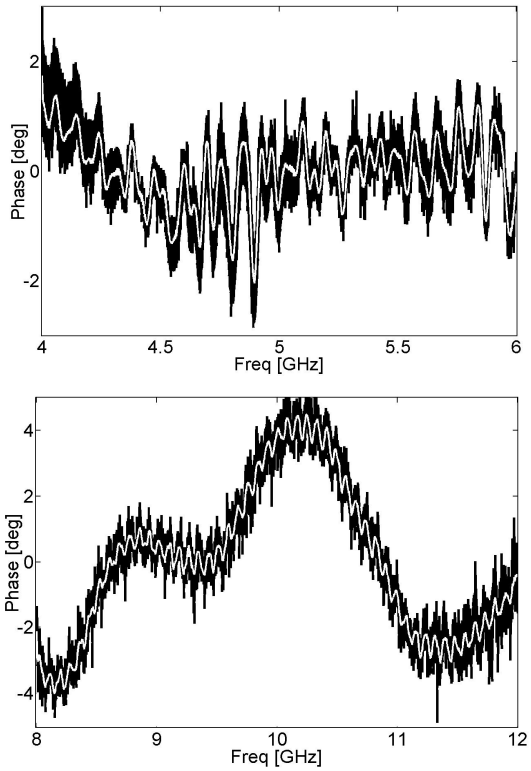

Fig. 3. The measured deviations of the RF phase from a linear dependence on frequency. The results for the 32 RF links are superimposed to show the small deviations from the mean (white line). [5] © 2008,IEEE.

included a passive PTTD unit. An eight port, thin film optical demultiplxer (DeMux) was used to accomplish the wavelength-controlled TTD operation, as shown in the inset in Fig. 1. The input modulated light was sent through a circulator into the DeMux, where, depending on its wavelength, it was routed to a particular output port. A different length of fiber (having a highly reflective (~100%) silver coated tip) was spliced to each output port of the DeMux, with a predetermined increment from port to port. Thus, the returned light, emerging from the circulator into the photodetector (O/E), experienced a wavelength–controlled pure delay, which is practically dispersion-free. Extremely fast angle switching was achieved here using a commercial fast tunable semiconductor laser, with a rated switching time of 200 ns (between any two wavelengths on a 50-GHz grid, covering the wavelength range of 1530–1560 nm), maximum output power of +9dBm, and a measured RIN of less than -150 dB/Hz. See [5] for more details.

III. CW RF Performances Of the Beamformer

An RF vector network analyzer was used to characterize the RF transfer function of the beamformer. The analyzer output replaced the RF source in Fig. 1, while its input was connected to the output of the O/E converter of the measured channel. The forward transmission coefficient S_{21} was measured for all 32 (4×8) RF links. Fig. 2 plot the frequency dependent magnitude $|S_{21}(f)|$, of the system transfer function, for all 32 RF links superimposed. Since different average RF insertion loss was measured for the 25 (3×8+1) different optical routes, we subtracted the per-link frequency average of $|S_{21}(f)|$. Similarly, fig. 3 plot superimposed the frequency dependent phase $\angle S_{21}(f)$ for all 32 RF links after the linear phase, (which measures the routes delay), was subtracted.

In spite of the fact that the four channels were equipped with *different* (though of the same brand) demultiplexers, O/E converters and associated circuitry, both the magnitude and phase responses are practically independent of the channel tested. This high degree of inter-channel uniformity among the 32 RF links leads us to conclude that their only common component, namely: the E/O converter, is responsible for the ripples in the heavy lines of the figures.

The larger frequency-dependent ripples may be characterized by two frequency scales: The slow variations with respect to the RF frequency are attributed to the (off-the-shelf) integrated-optics modulator itself (most notably is the

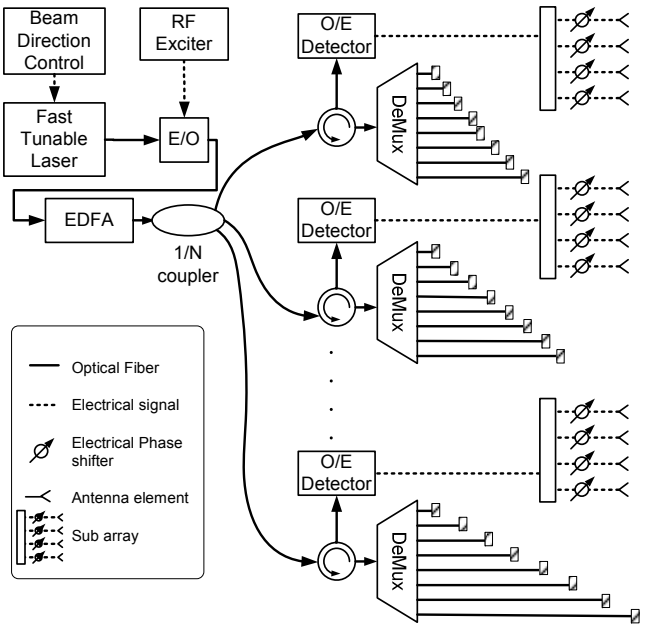

Fig. 4. Schematic drawing of a beamformer comprising N photonic TTD modules, each feeding a 4 element sub-array. [5] © 2008,IEEE

cutoff at ~11GHz), whereas the fast sinusoidal variations probably originated from the modulator driving circuitry and parasitic reflections. In principle, frequency domain fluctuations distort wideband pulse transmission and are thus highly undesirable. However, the obtained ripple performance of less than 0.4dB in magnitude and less than 4deg in phase should guarantee that performance even for signals wide enough to cover the entire band of operation (up to 20% of fractional bandwidth) is unhindered. Even better, the very similar behavior of all RF links in the beamformer of Fig. 1 makes it possible to calibrate out and 'flatten' the common ripples, represented by the heavy lines in Figs. 2-3 thereby achieving yet better RF performance.

IV. The Photonic Beamformer As a Building Block for Large Phased arrays

True time delay beamformers are of particular importance in large, wideband phased array antennas, having wide scan angles. While the PTTD building block of Fig. 1 exhibits very high performance, it seems expensive to feed each and every antenna element of a large array with such a device. Instead, a more attractive configuration, Fig. 4, may divide the large array into groups of subarrays. Each subarray, inherently small in size, may be of classical design, employing phase shifters. This series of subarrays will be fed, however, by a photonic beamformer of the architecture shown in Fig. 1. The inclusion of phase shifters also allows for overall calibration of the array, compensating for small delay errors in the PTTDs. In view of the excellent uniformity of S_{21} over wavelengths, *i.e.*, beam positions, calibration at a single wavelength appears sufficient. Note that a single control line, at the input of the laser tuning circuitry governs the angle scanning of the complete photonic beamformer. Moreover, a significant percentage of hardware can be remoted from the antenna itself, offering obvious advantages in difficult packaging situations.

V. Antenna Pattern And angle Tuning Performances

In order to establish the impact of the extremely smooth RF characteristics of the PTTD on the array performance, we'll simulate now the antenna pattern for an array comprising Q (=32) PTTDs of the design and characteristics of those described in Secs. II-III, each feeding a subarray of P (=4) phase shifters for a total of 128 radiating elements, operating in the X band and spatially spaced by a half-wavelength (d=0.015m @ 10GHz). The basic delay of the n-th PTTD is $n \cdot 50pS,\ n = 1..32$. Symmetric and bidirectional angle scanning can achieved by connecting the PTTDs to their corresponding subarrays with cables (e.g., an optical cable between the circulator and the E/O, or an electrical cable between the E/O and the antenna element) of unequal lengths, providing unequal wavelength-independent delays, $\tau(n), n = 1,..Q$, for the different subarrays. Thus, if these delays obey $\tau(n) - \tau(n+1) = 175pS, n = 1,..(Q-1)$, sequential transmission at λ_1 to λ_8 (at λ_1 all PTTD provide the same delay) will result in the following range of scan angles $[-61^0\ -39^0\ -22^0\ -7^0\ 7^0\ 22^0\ 39^0\ 61^0]$, derived from the formula $\arcsin((n \cdot 50pS - 175pS) \cdot c/(4d))), l = 0...7$. At these scan angles, diffraction limited patterns can be achieved at the center frequency $f_0 = 10\text{GHz}$ by adjusting the phase shifters not only to tune the subarrays to the right scan angle but also to compensate for inaccuracies in the time delays of the PTTDs. However, as the carrier frequency scans a bandwidth of 1GHz around f_0, the phase shifters give rise to parasitic lobes, whose strength increases as the number of PTTDs decreases.

Plot (a) in Fig. 5 describes the radiation pattern of the array at the extreme angle of 61°, assuming Hamming weighting of the 128 elements and taking the maximum radiation intensity at each angle as the carrier frequency scans the range of 9.5GHz-10.5GHz. It is further assumed that all delay lengths are perfect multiples of 50pS and that all 32 PTTDs share the same RF transmission characteristics over the 9.5-10.5GHz frequency range. The plot clearly shows a narrow diffraction-limited main lobe, accompanied by unwanted, though -20dB weaker, quantization lobes [9]. Had we assumed the array to comprise 128 PTTDs, the same main lobe would have resulted but without quantization lobes. The dashed line is the radiation pattern for an array comprising 128 phase shifters. While such an array produces a diffraction-limited beam in the broadside (0°) direction, its wide-band (1GHz) performance at 61° is quite poor, producing a beam much wider than that obtained from the photonic beamformer, albeit without the quantization

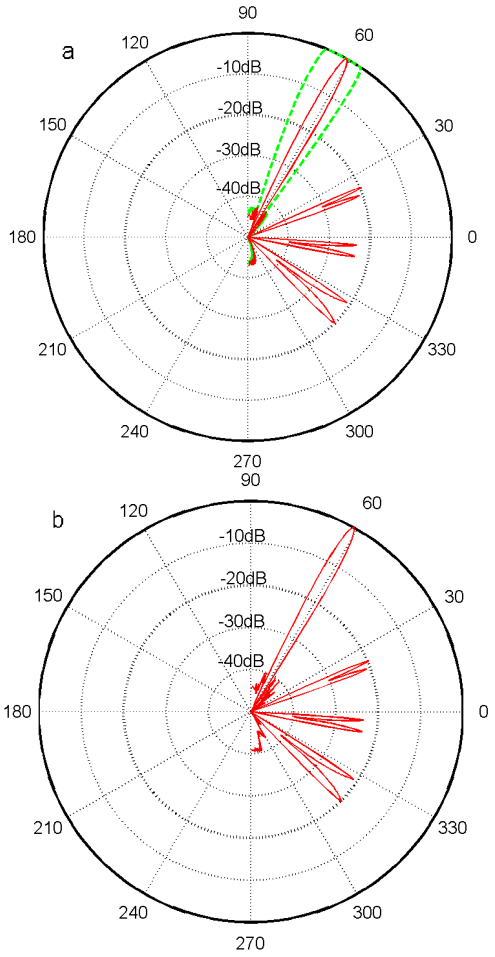

Fig. 5. Antenna patterns for a simulated antenna of 32 PTTDs, each feeding a subarray of four phase shifters. (a) Solid line: the envelope of radiation patterns of an error-free 32×4 array, aimed at 61 , as the carrier frequency covers 1 GHz around 10 GHz. The dashed line is the corresponding curve for an array comprising 128 phase shifters. (b) Same as (a) but including errors in the time delays of the PTTDs, as well as nonuniformities among the 32 PTTDs, see text. [5] © 2008,IEEE.

errors. Plot (b) for the 32X4 beamformer is the same as plot (a) except that two kinds of errors are now included: (a) it is assumed, following the unavoidable experimental situation of small errors in the implemented delays, that the built-in delays of the PTTDs have an additive random error of ~5pS rms (as mentioned earlier this error can be compensated for only at the center frequency f_0, by proper adjustment of the phase shifters); and (b) there exists non-uniformity among the $S_{21}(f)'s$ of the 32 PTTDS. This effect has been taken into account by ignoring the magnitude non-uniformity and by assuming a random phase error among the PTTDs and over the relevant frequency range of 0.5° rms. The results show very little degradation.

VI. RF Nonlinearities Introduced by the Photonic Link

The demonstrated beamformer, despite its excellent CW performance, is not exempt from introduced RF nonlinearities, contributed by the electronic to optical converter and to some extent by the optical to electronic converter. These converters, shared by any photonic link, may add to the system nonlinear budget, and the implications of their nonlinear behavior to both single and multiple frequency signals have been studied in detail [1,2]. Below, we investigate the effects of third-order nonlinearities, resulting, for example, from Mach-Zehnder modulators or other E/O and O/E converters, on photonic beamformers, which use linear frequency modulated waveforms [4] of the form:

$$V_{LFM}(t) = A\cos\left[2\pi f_0(t-t_0)+\alpha(t-t_0)^2\right]\mathrm{rect}\left[(t-t_0)/T\right] \quad (1)$$

where t_0 and f_0 are the pulse center time and frequency, respectively. $\alpha = \pi B/T$, where B is the total bandwidth of the signal (~GHz), and T is the pulse length (~tens of microseconds). During the pulse lifetime $(-T/2 \le t \le T/2)$, the instantaneous frequency $f(t) = f_0 + (B/T)\cdot t$ linearly scans the frequency range: $f_0 - B/2 \le f \le f_0 + B/2$.

When a Mach-Zehnder modulator (MZM) is used to convert the RF voltage, $V(t)$, to optical power modulation, $P_{opt}(t)$, its transfer function can be expressed as (when properly biased to remove even harmonics):

$$P_{Opt}(t) = \frac{T_{FF}P_I}{2}\left[1+\sin\left(\frac{\pi V(t)}{V_\pi}\right)\right] \xrightarrow{\text{AC terms to third order}} \frac{T_{FF}P_I}{2}\left[\frac{\pi V(t)}{V_\pi}+\frac{1}{6}\left(\frac{\pi V(t)}{V_\pi}\right)^3\right] \quad (2$$

P_I is the input DC optical power, T_{FF} is the optical insertion loss of the modulator, and V characterizes the sensitivity of the modulator to input voltage changes. $P_{opt}(t)$ contains a significant third-order nonlinear term, resulting in a fairly low input third-order intercept voltage [2], $V_{TOI} = 2\sqrt{2}\,V_\pi/\pi$. In transmit, a single LFM pulse passes through the beamformer on its way to the antenna, and as a result of the mapping between the instantaneous frequency and time during the pulse duration [4], any existing nonlinearity of the RF to RF transfer function will only produce out-of-range harmonics but not inter-modulations. Thus, the link can properly work with input RF voltages as high as $0.5V$, where the sine function saturates. In receive, however, the antenna element feeding the MZM, collects echoes from a few, if not many, close-by targets, giving rise to an input voltage to the MZM comprising a sum of several partially overlapping LFM pulses. Third-order nonlinearities will produce phantom targets, indistinguishable from the real ones, thereby reducing the achievable contrast of imaging systems.

VII. The Inter-modulation Products of Two LFM Echoes

When matched-filter processing [4] is applied to a sum of overlapping LFM echoes, system nonlinearities might cause the appearance of phantom targets. In order to analyze this effect for multiple reflection returns of LFM signals, we first consider the simple case of two echoes returning from two point targets with delays t_1 and t_2, ($t_2 > t_1$), with respective amplitudes r_1 and r_2. The received voltage signal will then be:

$$\begin{aligned} s_{rec}(t) = \; & r_1 \cdot \mathrm{rect}\left(\frac{t-t_1}{T}\right)\cos\left[2\pi f_0(t-t_1)+\alpha(t-t_1)^2\right] \\ & +r_2 \cdot \mathrm{rect}\left(\frac{t-t_2}{T}\right)\cos\left[2\pi f_0(t-t_2)+\alpha(t-t_2)^2\right] \end{aligned} \tag{3}$$

Expanding the overall transfer function of the beamformer, (prior to compression), in a Taylor series up to the third Ac term, $s_{out} = as_{rec} + bs_{rec}^3$, and examine only the inter-modulation products that fall within the system bandwidth, [f_0 – B/2 • f • f_0 + B/2], we see the emergence of 2 spurious LFM signals, , shown in Fig. 6.

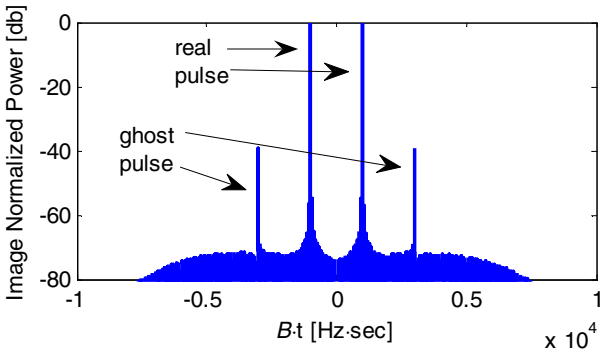

Fig. 6. Inter-modulation products of two LFM echoes after passing in the nonlinear transfer function of (2). T=10μsec, B=1GHZ, f_0=10GHz, temporal distance between the received echoes t=2μsec.

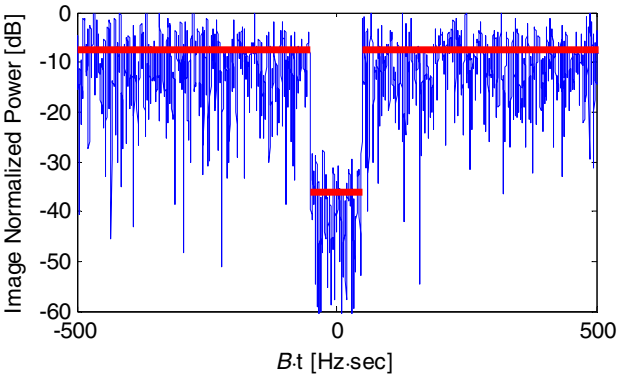

Fig. 7. The simulated instantaneous received power, from a zero-scattering narrow river sitting between two wide banks. Horizontal heavy lines measure the average power. Modulation index, m =0.5

VIII. The Effect of LFM Inter-modulation Products in a Multiple Return Scenario

To examine the case of multiple returns let's assume a zero reflecting river bounded by its two banks. We'll model the surface of the river banks as a manifold of randomly distributed scatterers, each returning the incident LFM pulse with a random delay. The received voltage signal will be given by the sum of many overlapping echoes from the river banks, but not from the river itself, resulting in an infinite contrast between the river and its two banks, practically bounded by the system noise floor. It turns out, that even for a noise-free system, the river will nevertheless appear to be reflecting, partly due to the finite skirts of the impulse response; but more importantly because of third-order inter-modulation products of the type discussed in the previous section, originating from scatterers on the river banks, see fig. 7.

While the first, linear phenomena results in a power independent contrast $\langle P_{Banks,comp}\rangle / \langle P_{River,comp}\rangle$, third-order nonlinearities result in a fast shrinking contrast with increasing $\langle P_{rec}\rangle$. Thus, to maintain a required contrast, $\langle P_{rec}\rangle$ must be limited, compromising the available signal to noise ratio.

We have studied this effect via simulation and experiment using an LFM pulse with practical parameters, ($T = 10\mu\mathrm{Sec}$, $B = 1\mathrm{GHz}$, $f_0 = 10\mathrm{GHz}$). The resulting contrast ratio, $\langle P_{Banks,comp}\rangle / \langle P_{River,comp}\rangle$, was plotted as a function of the modulation index m:

$$m = \frac{\pi\sqrt{2}s_{rec}^{RMS}}{V_\pi} = \frac{4s_{rec}^{RMS}}{V_{TOI}} \tag{4}$$

(Note that for a sinusoidally modulated signal, m reduces to its common definition [8]).

The simulation results, appearing as the solid line in Fig. 8, showing that while for low values of m the river level is controlled by the skirts of the impulse response, larger values of m quickly cause the contrast to deteriorate at the expected rate of 40dB/decade. To maintain a contrast larger than 25 dB m should not exceed 0.5.

The experimentally obtained results appearing as asterisks, shows good agreement with the simulation results for high modulation indices (m > 0.6), and the m^{-4} dependence is clearly obeyed. For small modulation indices (m < 0.2), the river signal is dominated by system noise, and consequentially, the contrast decreases as m^{-2}, since only the banks signal is affected by the changing m.

Although the curves in Fig. 8 were drawn for $T = 10\mu\mathrm{Sec}$ and B=1GHz, further simulations have shown that the m^{-4} portion of the curves in Fig. 8 are quite insensitive to T and B. Note that the obtained contrast is on the order of the order of $20\log_{10}(64/m^4)$.

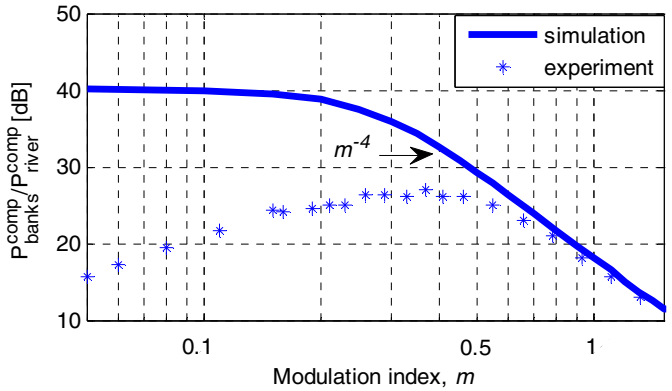

Fig. 8. Banks-river contrast as a function of the modulation index

X. Conclusion

With proper control of nonlinearities, photonic beamformers of the type described in this paper can perform well in both transmit and receive, over a very wide RF spectral range.

REFERENCES

* Dr. Oded Raz is currently an assistant professor at COBRA Research Institute, Eindhoven University of Technology, e-mail: o.raz@tue.nl

[1] C. Daryoush, A.S., Ackerman, E., Samant, N.R., Wanuga, S., and Kasemet, D,"Interfaces for high speed fiber-optic links: analysis and experiment", IEEE MTT Symposium Digest, 1, 297-301, 1991.

[2] Brian. H. Kolner and David W. Dolfi, "Intermodulation distortion and compression in an integrated electrooptic modulator", APPLIED OPTICS / Vol. 26, No. 17 / 1 September 1987.

[3] P. Lacomme, J.-P. Hardange, J.-C. Marchais, and E. Normant," Air and Spaceborne Radar Systems". Norwich, NY: William Andrew, 2001.

[4] M. Skolnik, Radar Handbook, 2nd ed. NewYork: McGraw-Hill, 1990.

[5] O. Raz, Sharon Barzilay, R. Rotman, and M. Tur, "Submicrosecond Scan-Angle Switching Photonic Beamformer With Flat RF Response in the C and X Bands", JOURNAL OF LIGHTWAVE TECHNOLOGY, VOL. 26, NO. 15, AUGUST 1, 2008

[6] O. Raz, R. Rotman, and M. Tur, "Wavelength-controlled photonic true time delay for wideband applications," IEEE Photon. Technol. Lett.,vol. 17, no. 5, pp. 1076–1078, May 2005.

[7] R. Rotman, O. Raz, and M. Tur, "Analysis of a true time delay photonic beamformer for transmission of a linear frequency modulated waveform," J. Lightw. Technol., vol. 23, no. 12, pp. 4026–4036, Dec. 2005.

[8] C. Cox, Analog Optical Links, Theory and Practice. Cambridge, U.K.: Cambridge Univ. Press, 2004.

[9] R. J. Mailloux, "Operating modes and dynamic range of active space-fed arrays with digital beamforming," IEEE Trans. Antenna Propag., vol. 54, no. 11, pp. 3347–, 2006.